Demulsification of crude oil emulsions tracked by pulsed field gradient NMR. Part I: Chemical demulsification

Tomas Nordeide Hjartnes[a*], Geir Humborstad Sørland[b], Sébastien Charles Simon[a*], Johan Sjöblom[a]

[a] Ugelstad Laboratory, Department of Chemical Engineering, Norwegian University of Science and Technology (NTNU), N-7491 Trondheim, Norway
[b] Anvendt Teknologi AS, Munkvollveien 56, 7022 Trondheim, Norway

*Tomas Nordeide Hjartnes, email: tomas.hjartnes@ntnu.no
* Sébastien Charles Simon, email: sebastien.c.simon@ntnu.no

Abstract

Emulsified water droplets must be extracted from crude oil for economical and transport purposes, which is achievable by chemical demulsification. Four different chemicals were tested on water-in-crude oil emulsions using a newly developed NMR method. Droplet size distributions were mapped at the beginning and end of experimentation. In addition, slice selections (soft RF pulses) were used to isolate the signal from residual droplets within the separated oil phase to study coalescence patterns in the emulsion bulk. The NMR could also return rapid continuous brine profiles for analysis of sedimentation rates and free water appearance kinetics. The residual water content was isolated by strong bi-polar gradient suppression, thereby allowing focus on the smaller droplets still emulsified in the top region in the brine profiles. Optimum concentrations were found for each chemical, and blends of several chemical demulsifiers were noticeably more efficient than the single component demulsifiers in this study.

1. Introduction

Crude oil contains many thousand different components. Among these there are several that contribute to stabilizing water droplets, such as asphaltenes, resins, crystallized waxes and naphthenic acids [1-3]. The two most polar components of crude oil are the asphaltenes and resins, which are considered to play a central part in the stabilization mechanism of water-in-crude oil emulsions. Asphaltene aggregates, solvated by resins, tend to form a viscoelastic layer at the oil-water interface, effectively stabilizing water droplets in the oil [4].

Emulsions are formed when two immiscible fluids, such as water and oil, are subjected to shear forces in the presence of a surface active agent. Different stages of crude oil production generates emulsions, as water is commonly injected to displace the reservoir fluids. Generation of emulsions may occur once the co-produced water and oil reaches chokes and valves in the processing pipes with large pressure differences. Two types of emulsions are encountered in the oil industry: Water-in-oil (W/O) and oil-in-water (O/W). The former is more frequently dealt with when producing the oil, while the latter is common in production water. In processing and transport, the drawback of having high water content in the oil is that it unfavorably compromises oil purity. High water content in oil is an issue since the standard for export quality requires it to have less than 0.5 % water [5]. Several methods of separation have been researched and adapted to the industry to meet this criteria.

Common separation techniques have been considered throughout literature, with the aim to reach sufficient levels of oil dehydration. These include: Gravity separation [6] chemical [7] and biological demulsification [8], liquid membrane separation [9], electrocoalescence [10] and microwave irradiation [11]. Among the aforementioned techniques, treatment by chemical demulsification is often seen as a necessity within the oil industry.

Emulsion treatment by chemicals can be separated into two categories: Non-emulsifiers and demulsifiers. The former is added to the oil as a preventive measure in order stop emulsions from forming, while the latter is added at a later stage to break an already existing emulsion [12]. Emulsion separation is a result of droplet collisions, promoting either coalescence, by drainage of the separating oil film, or flocculation of droplets, meaning permanent aggregation with thin oil films between them. Formation of flocs will increase the sedimentation rate. Understanding the flocculation kinetics is vital as it tends to follow the changes in emulsion properties, and usually precedes droplet coalescence [1]. Barrabino et al. [13] referred to the possibility of droplet interaction as an important factor that enhances droplet settling during demulsification in his experiments. Efficiency of a demulsifier, in a water-in-crude oil emulsion, has been shown to depend on the crude oil type, pH of the aqueous phase, salinity

and temperature [14]. Surfactants, polymers, solvents or chemical blends are typically used as demulsifiers for chemical separation. Since no chemical alone can achieve demulsification of every emulsion system, blends of various demulsifiers can be created with each component targeting specific characteristics of the emulsion [15]. Chemicals used as demulsifiers for emulsion breaking can be categorized into high or low molecular weight, each having different functionalities. Low molecular weight demulsifiers lowers the interfacial tension between water and oil, which indicates the demulsifiers' ability to adsorb to the the water/oil interface. High molecular weight demulsifiers (typically > 5000 g/mol) target alteration of rheology of the interfacial film by penetrating and modifying its properties [16].

Jones et al. [14] listed some of the main types of demulsifiers frequently used for industrial applications, all high molecular weight polymers. Two hydrophobic surfactants were compared in Jones' study, which showed that the ionic surfactant outperformed the nonionic surfactant. Sjöblom et al. [17] investigated stability of water-in-model oil systems with synthetic wax particles, where adding a mixture of fatty acid and amine provided the highest separation efficiency. The charged fatty acid/amine structure at the interface and a strongly hydrophilic film causes the stabilizing components to be replaced. The importance of surfactant monomer activity, for successful destabilization of an emulsion, was highlighted by Aveyard et al. [18] in a study of low molar mass nonionic and anionic surfactants in water-in-crude oil emulsions. The criticality of monomer activity was evidenced by an increasing rate of demulsification with increasing demulsifier concentration until the critical aggregation concentration (CAC) was reached. Urdahl et al. [19] investigated the destabilization of crude oil emulsions based on Norwegian Contintental Shelf oils, using hydrophobic ionic and nonionic surfactants, hydrophilic fluorinated surfactants and various polymers. The hydrophobic ionic surfactant, AOT, was more efficient than the nonionic analog. Promising results in emulsion destabilization were also found by Urdahl et al. in the use of fluorinated surfactants, which lower the interfacial tension, pointing towards the successful adsorption of surfactant on the water/oil interface, and possibly replacing crude components.

Nonionic polymers, often used for stabilizing oil-in-water emulsions, have shown destabilization effects for water-in-crude oil systems [20]. A comparative study of 14 water-soluble and 10 oil-soluble demulsifiers in crude oil emulsions was performed by Hajivand et al. [21]. These were accelerating the film drainage process, promoting aggregation and coalescence of water. The most efficient water resolution was achieved by fatty alcohol ethoxylate and triethanolamine. The research in Havajivands article indicate that the oil-soluble demulsifiers are better at resolving more water from petroleum w/o emulsions compared to that of water-soluble demulsifiers. Dendric polyether surfactants were tested in crude oil emulsions by Wang et al. [22], some of which reached separation efficiencies of over 90% v/v. The increasing ethoxylate content lead to increasing amounts of demulsified water, which also supports previous findings [18]. Adilbekova et al. [23] used a mixture of two nonionic block copolymers in kerosene for successful demulsification of water-in-crude oil systems (52% v/v). As the block copolymers are of amphiphilic nature, the hydrophilic and lipophilic segments can separately interact with the water droplets and the oil phase, respectively.

Emulsion destabilization, with related droplet coalescence and sedimentation rates, can be analyzed in various ways, where the most basic and extensively used technique is bottle testing [7, 21]. Multiple dynamic light scattering is another well established method used to study dynamic changes during demulsification [24, 25]. However, because this method relies on the ability of the infrared light to probe the dark crude oil, an alternative visualization method can be offered by pulsed field gradient (PFG) NMR. It is a fast and non-invasive technique to characterize and study emulsion stability, while probing the entire sample. The PFG NMR method was developed by Stejskal and Tanner to determine droplet size distributions, based on the principle of restricted diffusion of molecules within their colloidal structures [26]. It was used by Packer and Rees for water-in-oil emulsions, where the droplet size

distribution was assumed to be log-normal [27]. However, most work built on this assumption is limited when, for instance, dealing with bimodal distributions of droplet size. Characterization of crude oil emulsions, was first applied by Balinov et al. [28]. He applied the same NMR technique from Packer and Rees and validated it by comparing the NMR results with optical microscopy. Balinov also confirmed the Gaussian phase distribution approximation, which was previously the best available expression for calculating the echo attenuation of molecules experiencing a diffusion barrier.

Opedal further developed the method from Balinov et al. for determination of droplet size distribution of water-in-crude oil emulsions in PFG NMR, which reduced the overall acquisition time, shortening the length of each experiment down to approximately 5 minutes. Opedal validated the droplet size distributions obtained by NMR, with similar results to the distributions derived from microscopic investigation [29]. Simon et al. [30] showed that the water cuts for model emulsions, determined by NMR, were equivalent to the real, calculated water cuts. Similarities were also found between results generated by NMR and the Turbiscan in sedimentation rates and free water appearance kinetics. Sandnes et al. investigated the accuracy of the residual water content by Karl Fischer titration [31]. Sørland [32] implemented the spoiler recovery approach to the procedure by Opedal, shortening the acquisition time to under a minute, with no prior assumption of the shape of the droplet size distribution. The sequence spoils any directional magnetization in the sample within an external magnetic field, resulting in zero nuclear magnetization [33]. Then a delay, which is shorter than 5 times T_1, can be applied for producing a net magnetization. T_1 known as the longitudinal relaxation time, which is a decay constant for the relaxation of the nuclear spin magnetization in the z-direction. A delay shorter than 5 times T_1 allows for short experimentation times on unstable emulsions while minimizing the loss of NMR signal to noise.

The NMR procedure, used in this work, allows for droplet size distribution determination within a minute without any assumption on the shape of the distribution [32]. Other recent developments of NMR applied to crude oil emulsions involves the determination of the brine profile, i.e. measurement of the brine concentration (vol %) versus height of a column of settling emulsion. By determination of the brine profile at different times, the oil-water separation can be followed [34]. NMR procedures were also developed to measure the residual water content in the separated oil phase at the top after oil-water separation [31]. Studies have been performed with application of NMR on demulsification of crude oil emulsions by chemical demulsifiers [13].

Even if demulsification of crude oil emulsions have been the subject of numerous studies, limited work has been produced on the combination of demulsification methods. Our ultimate goal is to probe the interplay between chemical demulsification and electrocoalescence. The aim of this article will be to study the application of a new NMR method for characterization of coalescence, settling and separation of chemically treated water-in-oil emulsions. This article will be followed up by a second one, comparing separation induced by only demulsifier with that of combining demulsifier and electrocoalescence.

2. Methods and materials

2.1. *Chemicals and fluids*

A North Sea heavy crude oil was used throughout all the experiments. Relevant characteristics of this oil are provided in Table 1. Synthetic brine with 3.5 wt% NaCl was mixed together with the crude oil at 65 °C. Four demulsifiers were provided by AkzoNobel and NalcoChampion. Characteristics of the four demulsifiers tested are summarized in Table 2.

Table 1: Crude oil features for the North Sea heavy oil used throughout the experiments.

						SARA analysis [35]			
Density at 15 °C (g/cm^3)	Density at 65 °C (g/cm^3)	Viscosity at 65 °C (mPa·s)	TAN ($mg \cdot g^{-1}$)	TBN ($mg_{KOH} \cdot g^{-1}$)	Wat. cont.[a] (%)	Saturates (wt %)	Aromatics (wt %)	Resins (wt %)	Asphaltenes, Hexane insoluble (wt %)
0.939	0.906	20.4	2.15	2.81 $\pm$ 0.24	0.040	37	44	16	2.5

Density, TAN, TBN and SARA values are from Simon et al. [35]. [a] The water content was determined by Karl-Fisher titration.

Table 2: Demulsifier characateristics provided by manufacturers. MW: molecular weight. RSN: Relative solubility number, referring to the level of solubility of each chemical in water. Category refers to the level of environmental concerns related to the chemical (black, red, yellow, green). The green category includes substances on OSPAR's PLONOR list [36], and are presumed not to have a significant impact on the environment.

Chemical #	Category	Type	Chemistry	MW	RSN	Water solubility
1	ND	Drier	Blend	High	6.9	ND
2	Green	Dropper	Fatty acid alkoxylate ester	ND	9.5	Good
3	ND	Emulsion breaker	Blend	Medium	11.4	ND
4	Green	Dropper	Fatty acid alkoxylate ester	ND	6.1	Poor

ND = Not disclosed by manufacturer.

2.2. *Preparation of emulsion*

A cylindrical vial of volume 60 mL, and a diameter of 3 cm, was filled with 15 mL of brine and 15 mL of crude oil (50% v/v water cut) that were weighed. Then an Ika® Ultra-Turrax® T 25 disperser was used for a total of 2 minutes at 65 °C (in an oil bath) to prepare the emulsion by mixing. First, the sample was subjected to 3000 rpm for 30 seconds, while moving the dispersing element up and down, to make sure that brine was evenly distributed in the crude oil. Then the mixing speed was increased to 24000 rpm for 90 seconds more. Demulsifier was added by pipette from a stock solution (see Table S.3, supplementary materials) immediately after mixing before shaking the sample vertically 50 times. Right after distributing the demulsifier, a volume of 2 mL was pipetted from the 30 mL sample into a square glass vial for analysis in the NMR for 2 hours at 65 °C. The NMR sample height limit is around 2-3 cm, so the square glass vial was filled with 2 cm of emulsion. The remaining emulsion was put in a heating cabinet at 65 °C and its water content (in the emulsified phase) was analyzed in the NMR after 3 hours.

2.3. *Emulsion characterization by Low Field NMR*

The Pulsed field gradient NMR method, that the experimental work in this article is based on, has been validated by previously mentioned research in the introduction [30, 31, 34]. The low field NMR instrumentation for emulsion characterization is produced by Anvendt Teknologi AS (Norway). The magnetic field has a resonance frequency of 21 MHz, field strength of 0.5 T and maximum gradient

strength of 4 T/m. Emulsion samples studied in the NMR were approximately 20 mm in height and 10 mm wide. Direct air supply was connected to control the temperature of the sample throughout the experiments.

2.3.1. *The spin echo (SE) and stimulated echo (STE) sequences*

When characterizing an emulsion by low field NMR, signals from both oil and brine are simultaneously present. Thus, there is a need for isolating the signal from the water droplets without picking up any oil signal in order to study sedimentation kinetics, droplet sizes and remaining emulsified water content after demulsification. Two sequences are applied in these experiments for different purposes: The pulsed field gradient stimulated echo (PFGSTE) sequence (preparation sequence) and the pulsed field gradient spin echo (PFGSE) sequence (characterization sequence) as shown in Figure 1. The preparation sequence is applied to isolate the signal from the water phase, and depending on the parameters used one may isolate the complete water phase or just the water present in droplets, excluding any bulk water phase. The characterization sequence is then applied to extract characteristics of the emulsion, such as brine profile and droplet size distributions. More detailed information on the background theory can be found in the work which the methods in this paper are based on [29, 34].

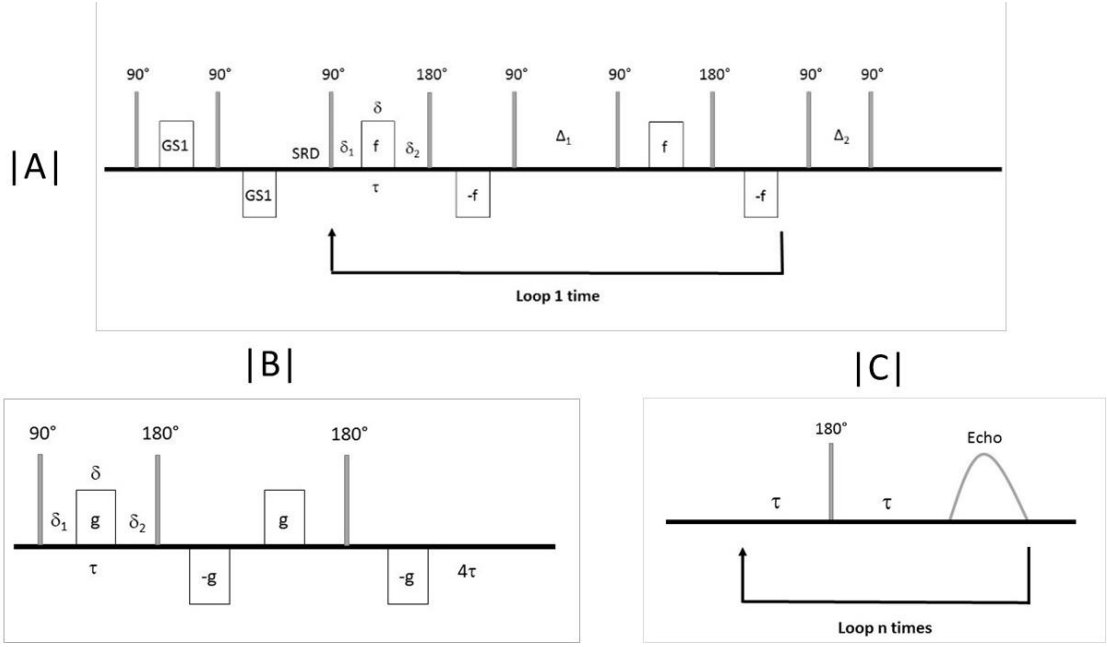

Figure 1: Sequences used to generate information from the emulsion sample. The preparation sequence consists of the |A| spoiler recovery, which induces zero magnetization in all directions, followed by the PFGSTE sequence, also known as the oneshot sequence. Next, the characterization sequences follow, which consists of the |B| PFGSE sequence or the |C| CPMG sequence.
Reprinted from "The application of pulse field gradient (PFG) NMR methods to characterize the efficiency of separation of water-in-crude oil emulsions.", Debora Salomon Marques, Geir Sørland, Simone Less, Regis Vilagines, Journal of Colloid and Interface Science, 512: 361-368, Copyright 2017, with permission from Elsevier.

A combination of the PFGSTE (|A| in Fig. 1) and the CPMG (|C| in Fig. 1) sequences are used to produce a T_2 distribution from water only or a T_2 distribution from both oil and water. T_2 is known as the transverse relaxation time as it is a time constant for the decay of the transverse spin magnetization (xy-plane) towards zero. Whether we are left with the water signal or both oil and water depends on the use of mono-polar or bi-polar gradients. When using weak mono-polar gradients, there is no suppression of bulk signal due to diffusion. Suppressing the crude oil signal then relies on the duration of Δ_1 (z-storage interval) due to significant differences in T_1 relaxation times between the water and oil. When switching to strong bi-polar gradients, and using the “asymptotic approach”, the

bulk signal (both oil and water) may be suppressed, leaving the emulsified water for further characterization. Between two applied pulses (as seen at the end of Fig. 1 |A|), an eddy current delay, Δ_2, is included to ensure that eddy current transients have adequately dissipated to not interfere with the acquisition of the NMR signal. A comprehensive list of parameter values used for the PFGSTE and PFGSE sequences can be found in Table S.1 (supplementary materials).

By applying the spoiler recovery delay (SRD in Fig. 1, |A|) prior to the PFGSTE sequence, the measurement time can be reduced significantly compared to previous work because the time does not need to be 5 times T_1 for having the system at thermal equilibrium before each scan. The spoiler recovery method uses two 90° RF pulses, where the phase of the second pulse is orthogonal to the phase of the first pulse, and a bipolar pair of magnetic spoiler gradients, GS1, of different shape and duration. δ is the duration time of an applied gradient, δ_1 is the time delay between a pulse and an applied gradient; and δ_2 is the time delay from the end of the applied gradient to the next pulse. **2**τ represents the inter-echo spacing (time between appearing echoes). A one-dimensional water profile can be obtained by combining the PFGSTE sequence and a profile sequence (see Figure S.2, supplementary material). The PFGSTE sequence is looped one time to suppress the crude oil signal, while the following profile sequence produces an echo during a read gradient, which is then Fourier transformed to generate a water profile [33].

2.3.2. *Droplet size distribution and slice selection*

When conducting measurements to retrieve the droplet size distribution, or the surface-to-volume profile (S/V-profile), the "short observation time approach" is used (Eq. S.1 and Eq. S.2 in supplementary materials) [33]. Diffusion measurements at short observation times reveal information regarding droplet geometry restrictions, which was made available when Mitra [37] developed a method for determination of the surface/volume and surface relaxation parameters. It was realized by simultaneously using data on the time-dependent diffusion coefficient and the net magnetization at short observation times.

The short observation time approach imposes no significant limitation on droplet sizes that the PFG NMR can detect. However, the deviation between the time-dependent restricted diffusion coefficient and the unrestricted bulk diffusion coefficient becomes smaller, which makes droplet measurements less accurate. Then the T_2 distribution will not reflect the real DSD in these experiments because the fast diffusion limit is assumed (Equation S.3, supplementary materials). Therefore, a correction is made, in experiments presented in this article, for large droplets by taking the T_2 bulk into account in the DSD distribution calculations. This T_2 correction poses a problem for the inverse Laplace transformation of the T_2 distribution as droplets get bigger (and their T_2 values longer), resulting in a distribution that stretches longer than the T_2 bulk value, generating negative droplet sizes for the longest T_2 values. The real limitation of droplet size measurements is then encountered in the accuracy of the T_2 distribution arising from the fast diffusion limit. The DSD measurement limitation can be solved by increasing the observation time of the experiments, allowing hydrogens to hit the boundary of the droplets more frequently.

Once a water layer has formed at the bottom of an emulsion sample towards the end of an experiment, measuring its droplet size distribution will give an overestimate of the droplet sizes, as the bulk phase is interpreted as big droplets. To circumvent this problem, bulk suppression by root of mean square displacement (RMSD) can be applied in the preparation sequence using bi-polar gradients and a rather long Δ-storage delay. Using this technique may also remove big droplets that exceed a certain size together with the bulk water. For this reason, shaped RF pulses in combination with magnetic field gradient has been applied to excite only a slice of the sample (Figure S.1,

supplementary materials) where the bulk water phase is excluded [38]. As the sample is 20 mm long and the water cut is 50%, the slice has been adjusted to target the upper half of the sample (while excluding the rest). In this way, the droplet size distribution can be measured for the separated oil phase, still with emulsified droplets left, while cutting out the free water layer at the bottom from the measurements entirely. This technique has been applied when determining the final droplet size distributions, at the end of each experiment, in this work. More detail on the determination of droplet size distribution (Eq. S.1-S.3), which parameters are used for the Laplace transformation (Table S.2), and how the slicing method is conducted (see Eq. S.4-S.6) can be found in the supplementary materials.

3. Results

3.1. *Development of NMR procedure for chemical demulsification studies*

This section will present how the NMR method is used for analysis of chemical demulsification of crude oil emulsions. All results presented consist of measurements ranging from 2-4 parallels per data point (each data point is the average value over these experimental parallels), with errors calculated based on minimum and maximum values for all curves unless otherwise stated below the figures. As chemical 1 showed greater efficiency in the screening amongst the tested chemicals, this will be presented to validate the specific NMR technique used throughout the experiments.

Upon deciding which concentrations to use for chemical 1 in the PFG NMR, similarly to the other chemicals that will be presented, concentration sweeps were performed by bottle testing in a heating cabinet at 65 °C. Two to three concentrations were tried, and whichever concentration yielded some visible droplet sedimentation, or free water layer the bottom of the sample, determined which concentration to be experimentally analyzed by NMR. In the second results section, comparison will be made from chemical 1 to chemical 2, 3 and 4.

Four concentrations were used from chemical 1, each with several parallels: 5 ppm (4 parallels), 10 ppm (4 parallels), 20 ppm (2 parallels) and 50 ppm (2 parallels).

3.1.1. *Effect of chemical 1 on droplet size distribution*

The oil-water separation was performed at a temperature of 65 °C. This temperature allows for reduction of the viscosity of the crude oil to a value (20 mPa·s) which is relatively similar to the oil treated in industrial separators [10]. A 50% water-cut (v/v) crude oil emulsion without demulsifier was studied for 2 hours with no sign of sedimentation, nor coalescence, mostly due to the high concentration of asphaltenes, resins (Table 1) and small droplet sizes.

The initial (t = 0) droplet size distributions have been normalized against maximum intensity and compared for different concentrations of chemical 1 (Fig. 2). The black dotted line is the initial DSD for emulsion without the presence of demulsifier, which has a mode of 7 μm in diameter. It represents the baseline for the subsequent demulsifier experiments. For 5-10 ppm there is a slight shift in the mode of the curves, indicating that droplets have immediately coalesced in the emulsion bulk after demulsifier addition, even at these lower concentrations. Increasing to 20-50 ppm, a much wider DSD is observed as demulsifier is reaching a greater number of droplets, promoting more small droplets into larger droplets than the lower concentrations by coalescence. Such initial rapid effects of demulsifier on the system, leading to large shifts in DSDs, was also reported by Opedal et, al. [29].

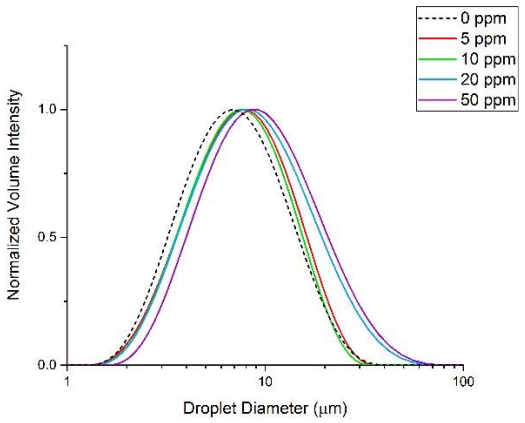

*Figure 2: **Initial DSD** for each concentration from chemical 1 from 0 to 50 ppm, where a representative parallel has been plotted for each concentration.*

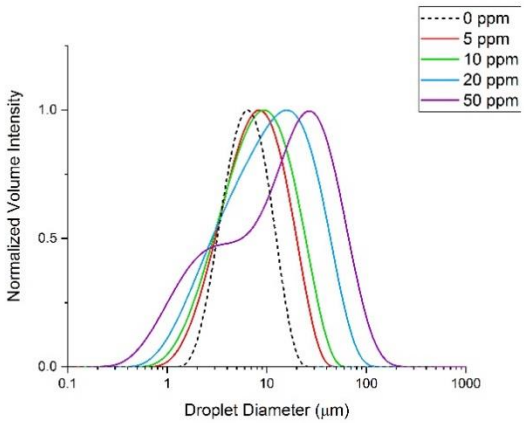

*Figure 3: **Final DSD,** i.e. after 2 hours of separation, for each concentration from chemical 1 from 0 to 50 ppm, where a representative parallel has been plotted for each concentration.*

As previously mentioned, slice selections can be performed by NMR on the samples to extract information from regions of particular interest. In our case, it is vital that the bulk water at the bottom is taken out of consideration when measuring the final droplet sizes, thereby avoiding any artefacts. The same samples as shown in Figure 2 have been measured again after 2 hours (Fig. 3) by applying slice on the region comprising the middle to the top of the sample to avoid the presence of free water.

We can clearly see the modes shift and the DSDs widen, which is also evidenced by increased average droplet size (Fig. 4) and wider DSD at 30% of maximum normalized intensity (Fig. 5) with increasing concentration of demulsifier. The DSD has a shift both towards smaller and larger droplets. The smallest droplets appearing is likely due to an artefact that sometimes results from the inverse Laplace transformation, depending on signal-to-noise and the curve smoothing factor applied [39]. The smoothing factor has a tendency to stretch the DSD towards smaller and bigger droplets when decreased, which is not real, especially considering that the final DSD shows smaller droplets (Fig 3.) than the initial DSD (Fig. 2). However, there is a real possibility of small droplets appearing as Yeung et al. [40] showed that micrometer-sized droplets can detach from the surface of larger droplets when covered by high concentrations of bitumen. In any case, small droplets are left at the top as bigger droplets sediment out of the top emulsion region (Fig. 3), leaving the small stable droplets behind unable to coalesce. Overall results presented in Figure 4 confirm the continuous coalescence of droplets in the oil phase. Even though flocculation is expected to occur, it will likely not affect the droplet size measurements, as the DSD is based on the random diffusion of water molecules inside the confines of a droplet. As long as the aggregated droplets remain separated, the molecules will only hit the wall of the droplet which encapsulates it. Because of this droplet boundary, the DSD will represent these droplets as separate, unaffected by flocculation.

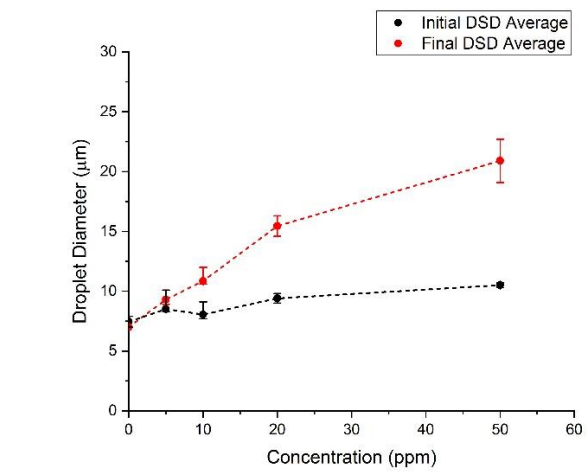

Figure 4: ***Initial and final (after 2h) DSD average****, with droplet diameter (µm) vs. concentration of chemical 1 (ppm). Each data point consists of the average over two parallels for both curves. Error bars represent the maximum and minimum values at each concentration.*

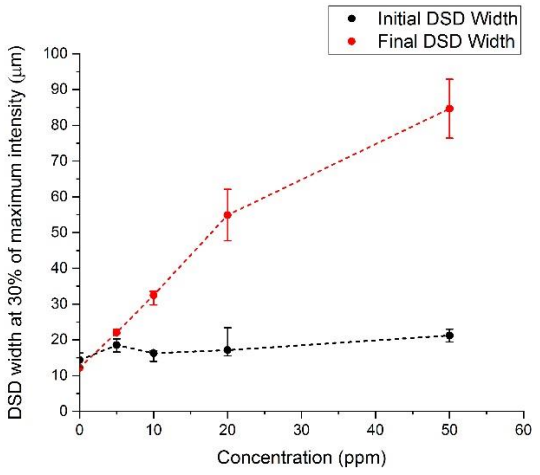

Figure 5: ***DSD width at 30% maximum normalized volume intensity*** *vs. concentration of chemical 1 (ppm). Each data point consists of the average over two parallels for both curves. Error bars represent the maximum and minimum values obtained at each concentration.*

3.1.2. *Brine profile for chemical 1*

1) Sedimentation rate

After addition of demulsfier, the NMR can track the stability of the emulsion by continuously scanning and supplying a brine profile every 49 seconds. The brine profile simply shows the water content (vol. %) related to specific positions within the crude oil emulsion sample (see Figure S.3, supplementary materials). As a material balance check, the area under the brine profile is calculated before and after the experiment (which should be unchanged), giving us values close to 50% water in all the systems tested. By combining all profiles (see Figure S.4, sup. mat.) throughout the on-going water-oil separation experiment into iso-volumetric curves (see Figure S.5, sup. mat), sedimentation rates can be calculated. An example calculation is shown in Equation S.7 in the supplementary materials. The possibility of calculating the sedimentation rate is under the presupposition that there is an existing sedimentation front in the evolution of brine profiles. For chemical 1, sedimentation fronts have been observed, except at the lowest tested concentration of 5 ppm. Therefore, calculated experimental sedimentation rates have been compared against values from the theoretical Stokes' equation for droplet velocity (Table 3), which is shown in Equation 1 [1]:

$$v = \frac{d^2 g|\Delta\rho|}{18\mu}, \qquad |1|$$

where d is the droplet diameter, g is the gravity constant, Δρ is the density difference between dispersed (water) and continuous (oil) fluids, and µ is the viscosity of the continuous phase (oil). In the case of a polydisperse system, the choice of d for Equation 1 is ambiguous. In this article we have chosen to use the average volume based drop diameter determined right after demulsifier addition (Fig. 2) for the calculation of the Stokes' sedimentation rates. Further explanation and example calculations can be found in the supplementary material (Fig. S.3-S.5 and Eq. S.7). The comparison in Table 3 presents the experimental velocities for the concentrations in which a sedimentation front has been observed, which is the case for all concentrations, except 5 ppm. The experimental values are higher than the theoretical Stokes values by two orders of magnitude in all cases. Moreover, Stokes' law considers diluted systems: Typically, sedimentation rate decreases when the dispersed phase

concentration increases (hindered sedimentation) [41], which accentuates the difference between Stokes' rate and measured sedimentation rate. This is the opposite of what is observed in this study where the experimental sedimentation is higher than predicted from Stokes. Discrepancies between measurements and values calculated from Stokes' law has also been found in previous work [13], where the results did not point to any relation between sedimentation rate and the square of the droplet radius, as indicated by Equation (1).

Table 3: *Comparison between experimental and Stokes' sedimentation rates (chemical 1). Uncertainties represent the minimum and maximum values obtained.*

Concentration (ppm)	**$V_{experimental}$ (mm/s)**	**V_{stokes} (mm/s)**	**V_{exp}/V_{stokes}**
10	$1.85 \cdot 10^{-2} \pm 4 \cdot 10^{-3}$	$1.96 \cdot 10^{-4} \pm 3 \cdot 10^{-6}$	94
20	[a] $2.00 \cdot 10^{-2}$	$2.18 \cdot 10^{-4} \pm 3 \cdot 10^{-6}$	92
50	$2.85 \cdot 10^{-2} \pm 5 \cdot 10^{-3}$	$2.97 \cdot 10^{-4} \pm 2 \cdot 10^{-6}$	96

[a] No uncertainty available as this was the only parallel for which sedimentation rate calculation was possible, as the first two brine profiles were not recorded.

In addition, Stokes' equation assumes monodisperse droplets, when in reality our w/o system is polydisperse as seen from the initial droplet size distributions (Fig. 2). The difference can also be explained by the rapid coalescence in the emulsion bulk, which further increases the spectrum of small to large droplet sizes. Droplets can also flocculate, leaving droplets on the verge of coalescence, which accelerates sedimentation.

2) Free water

Similarly to the already mentioned estimation method of sedimentation rate, an iso-volumetric curve can be also be constructed for free water appearance. The free water layer height has been plotted against time for increasing concentration of demulsifier (Fig. 6). The free water curves were determined from brine profiles by considering that the part of the profile with WC > 80% v/v, which corresponds to free water. The value of 80%, and not 100%, was used since oil would stick to the glass walls of the emulsion sample at the bottom, lowering the NMR water signal in this part. The effect of concentration on the free water appearance kinetic is shown, in which an increasing concentration of demulsifier speeds up the formation of free water, as evidenced by the large difference in going from 5 ppm (red) to 10 ppm (green). At 50 ppm the curve levels off even faster, making it difficult for the NMR to detect as many points. All curves in the figure reach a plateau close to 40% of the sample height, which could indicate that that this is the water separation limitation of chemical 1 in regard to this specific w/o emulsion system. Reaching this limit means that a significant amount of water is still emulsified at the end of separation.

In order to characterize the coalescence rate, it was initially attempted to determine the coalescence rate by fitting the initial variation of the free water content as a function of time with a linear regression. However, some of the data provided a poor fit and therefore this attempt was excluded. Instead, the parameter of free water appearance time, i.e. the initial time at which the free water content is higher than zero, was determined (from data in Fig. 6) to characterize the kinetic of the free water appearance, since this was reproducible.

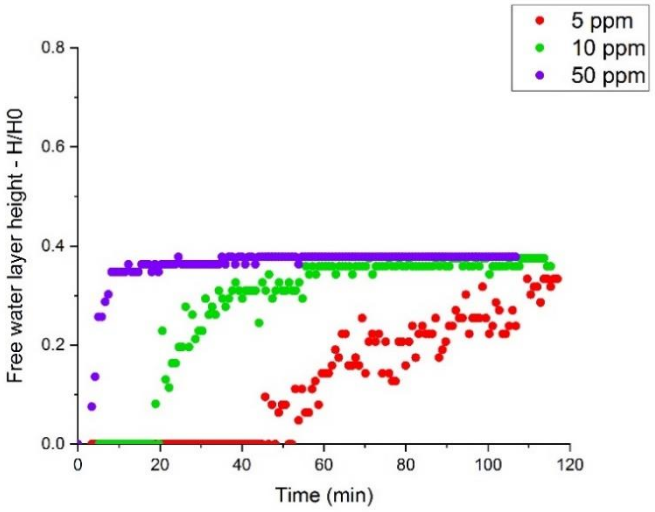

Figure 6: ***Free water layer height (H/H₀)*** *vs. time (min) for increasing concentrations of demulsifier. The curves range from 5 ppm (red), 10 ppm (green) and 50 ppm (purple). Representative parallels have been chosen for the concentrations shown.*

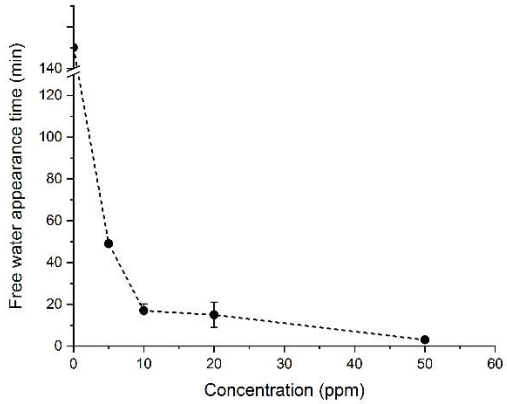

Figure 7: ***Free water appearance time (min)*** *for different concentrations from 0 to 50 ppm of chemical 1.* The data points represent an average of the parallels with error bars showing the maximum and minimum values.

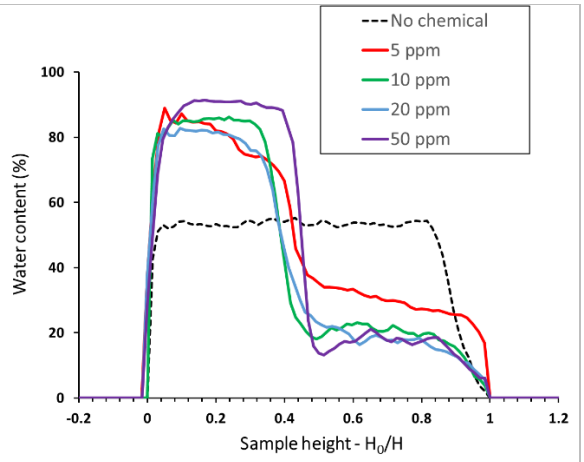

Figure 8: ***Final brine profiles*** *for different concentrations from 0 to 50 ppm of demulsifier. Water content (%) vs. normalized sample heigh, H/H₀. A representative parallel was chosen for each concentration.*

The free water appearance time (Fig. 7) between 10-20 ppm is very similar. The decrease of free water appearance time, with concentration of chemical 1, becomes very small above 10 ppm. Raising the disage above 10 ppm to speed up separation could become uneconomically feasible, since additional water resolution is limited. The final brine profile plot against normalized sample height (Fig. 8) shows how the water profile has changed after 2 hours of separation with rising concentration in relation to its initial starting point (black dotted line). Bulk water can be observed as a large peak in the bottom half of the sample, while the emulsified droplets remains at the top, in the separated oil phase. The final brine profiles (Figure 8) allows determination of the free water content as shown before (Fig. 6), as well as the residual water content. Water content is relatively constant in the top phase part of H/H_0 from 0.5 to 0.8, after which point the water content to drops significantly. For the purpose of

comparison, the water content at 75% of the height of the emulsion sample was logged and plotted (Fig. 9) as a function of the demulsifier concentration.

Residual water from the 30 mL sample, from where the 2 mL NMR samples are collected, is shown in black in Figure 9. In the same figure, the water content from the 30 mL sample (red) was cross-checked with the emulsified water from the 2 mL samples (blue), as well as the water content at 75% height of residual brine profile (black). The emulsified water curve (blue) is the upper part of the earlier shown brine profiles (Fig. 8), and is the percentage of water left after the NMR has suppressed the bulk water signal at the end of the experiment. All curves show similar trends where maximum efficiency of chemical 1 seems to be reached at around 10 ppm, at which point further increasing the dosage is ineffective at inducing higher separation. However, it can be noted that the water content is high even after the highest demulsifier concentration (≈20% v/v). The reason for partial settling of droplets is not completely understood as sufficient information about the chemicals have not been disclosed, but other demulsification literature has reported on the appearance of demulsifier concentration thresholds [42, 43]. These cases are attributed to irreversibly adsorbed asphaltenes at the droplet surface so that demulsifier molecules are unable to reach full surface coverage. The emulsified water content is significantly lower than the two other curves (top half 30 ml sample and 75% of H/H_0). The procedure to determine the emulsified water content eliminates the signal from the bulk water, but also from the bigger water droplets. The region containing lower water content would therefore correspond to the smallest range of droplets where the diameter is approaching a certain detection limit. This droplet size limit, as mentioned in Section 2.3.2, depends on the fast diffusion limit as part of the short observation time approach. Since the PFG NMR will only calculate the mean droplet size with certainty, the range of droplet sizes displayed in the DSD can only be used to determine whether or not there has been a droplet increase throughout the experiment, as well as sample position of such big droplets.

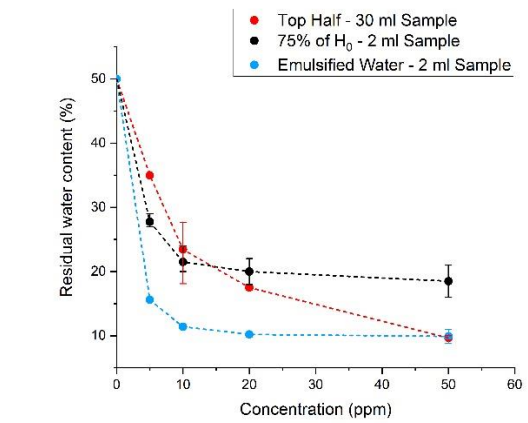

Figure 9: ***Residual water content (%) of emulsion*** *vs. concentration of demulsifier. Top half of 30 ml sample (red) represents the rest emulsion. Each point of the red curve is one parallel except for 10 ppm (average of two points). The 75% of initial height (black), H_0, is also a measure of rest emulsion. Each point of the black curve is an average of two points. Emulsified water (blue) is the remaining water content after bulk suppression of the 2 ml sample. Each point of the blue curve is one parallel.*

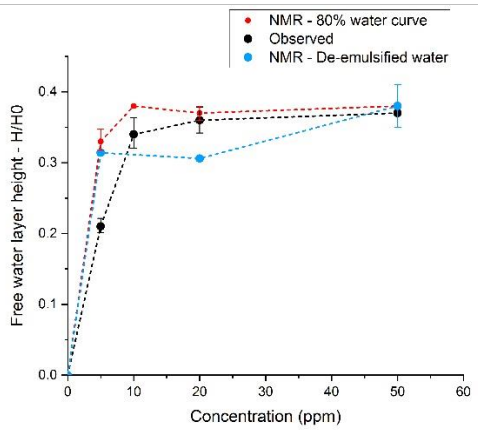

Figure 10: ***Free water layer height, H/H_0,*** *vs. concentration of demulsifier. Observed (black) are values visually measured after 3 hours of NMR analysis. Each point of the black curve is an average of two parallels. 80% water front (red) is the iso-volumetric curve of 80% water content, which represents free water. Each point of the red curve is an average of two parallels. De-emulsified water (blue) is the initial brine profile area less the emulsified profile area. Sometimes the initial water content is slightly under 50% so that the de-emulsified curve does not mirror the emulsified curve exactly. Each point of the blue curve is one parallel, except for 50 ppm which is the average of two parallels.*

Figure 10 displays the free water layer height against concentration of demulsifier. To help validate NMR results, the free water layer (black), determined from visual inspection of the sample, has been cross-checked against the end-point of the iso-volumetric curve of 80% water content (red), which is the criteria for free water. It appears that the NMR data fits the observed data quite well. De-emulsified water (blue) is the initial water cut of 50% less the emulsified water from Figure 9 (blue). Since some values of the initial water content are slightly less than 50% in some cases, the de-emulsified curve does not perfectly mirror the emulsified curve. We can again observe that these curves (Fig. 10) reach a plateau around 10 ppm, where further development in demulsification ceases. In other demulsification studies [44], sufficient residence time has been mentioned as one of the crucial factors to allow a chemical to successfully separate the dispersed water from the oil. Because the results from the chemical 1, studied in this article, shows signs of rapid bulk coalescence and sedimentation, limited time is available for the smaller droplets to coalesce with the big droplets. The fast droplet coalescence in the bulk, which yields a sedimentation threshold, is consistent with the final brine profiles (Fig. 8) where the emulsified water content is more or less constant at 20% once a certain dosage is reached.

3.2. *Comparison with chemical 2, 3 and 4*

In this section, comparisons are made between the data obtained from droplet size distributions and brine profiles for all the different chemicals. Several concentrations have been used to capture trends arising from a gradual increase of dosage, and its effects on the separation efficiency, both in terms of free water layer height and the rate of separation.

3.2.1 Effect of each chemical on the droplet size distribution

Optimal concentrations have been selected for chemicals 1-4 (Fig. 11), based on the performance of the various concentrations used in experiments, and their respective DSDs have been plotted. When there is no further significant improvement of separation at a certain concentration, it is considered optimal. The width of the DSDs for chemical 1 and 2 are the same, meaning that the distribution of droplet sizes are similar. However, the intensity of the curves are different, thus the amount of droplets are less in the top phase for chemical 1 compared to chemical 2. Chemical 4 has a DSD that stretches further than 1 and 2, towards larger droplets, and has the highest volume intensity of all the chemicals. Even bigger droplets are left when using chemical 3, seen from its long tail, for which the lowest volume intensity of all the chemicals is observed. Low intensity indicates that there are fewer droplets in the top, even though they are generally bigger than for the rest of the chemicals. While the DSD for chemical 3 stretches further than these values, it is likely due to the chosen smoothing factor that results in an unreal width. However, this large tail points towards the presence of very large droplets in the presence of demulsifiers.

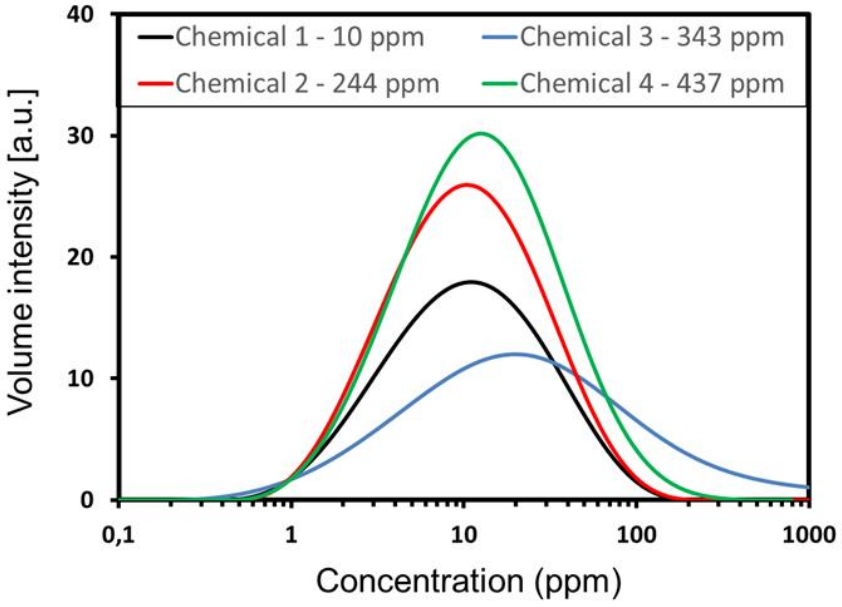

Figure 11: ***Final DSD (after 2 h)*** *for chemicals 1-4, plotted as volume intensity of emulsified droplets vs. concentration of the chemicals. The optimal concentrations, at which point no significant separation improvement occurs if demulsifier dosage increases, have been plotted for each chemical. The same smoothing factor (=5) and number of scans (=16) has been used for all the presented distribution curves to ensure comparability.*

3.2.2 Brine profile comparisons

To check whether or not there are sedimentation fronts existing during the separation process for a specific concentration of the chemicals, several brine profiles are plotted together at various time steps in Figure 12 (a)–(d). Chemical 1, at a concentration of 10 ppm, has a clear piston-like movement of water droplets from the top of the emulsion towards the bottom. This piston phenomenon is not present for chemical 2 at 244 ppm or chemical 4 at 437 ppm, as the water content is the same from the mid-point of the emulsion towards the top. Chemical 3 does not display a piston, but has a gradient of water content, which is decreasing from the mid-point, across the sample and towards the top. Based on the observations from Figure 12 (a)-(d), it seems that there is a relation between the shape of the curve in the topmost part of the sample and the final percentage of water resolved. Sedimentation occurs at a greater speed and has a higher final water resolution for chemicals 1 and 2, which have piston shapes and steep gradient shapes, respectively. Compared to chemicals 3 and 4, where the water content falls equally across the top part of the sample, the final percentage of water separated is much lower.

As it is not possible to define a clear sedimentation front for chemicals 2-4, sedimentation rates could not be calculated in order to assess the sedimentation of droplets during oil-water separation for chemicals 2, 3 and 4.

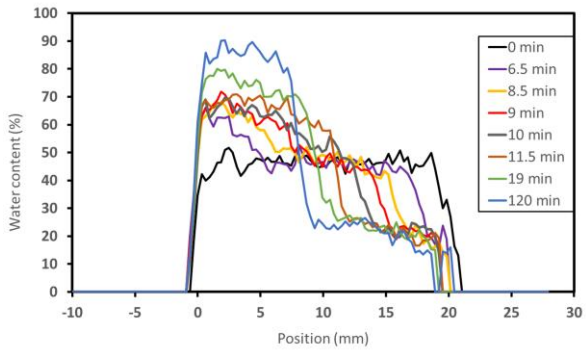

Figure 12 (a): Brine profile measurement at different times in the presence of chemical 1 at 10 ppm (optimal concentration).

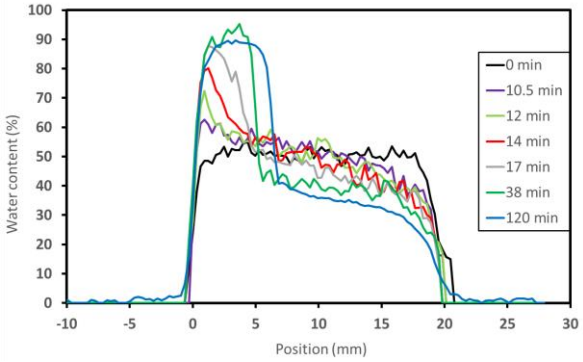

Figure 12 (b): Brine profile measurement at different times in the presence of chemical 2 at 244 ppm (optimal concentration).

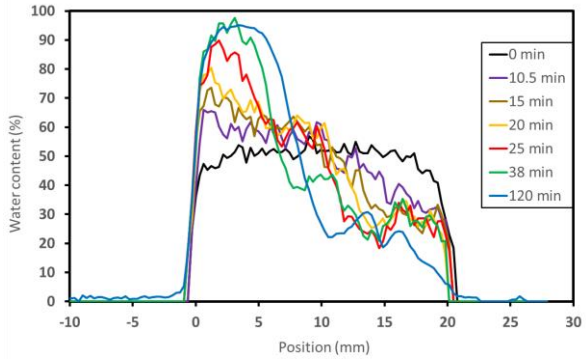

Figure 12 (c): Brine profile measurement at different times in the presence of chemical 3 at 343 ppm (optimal concentration).

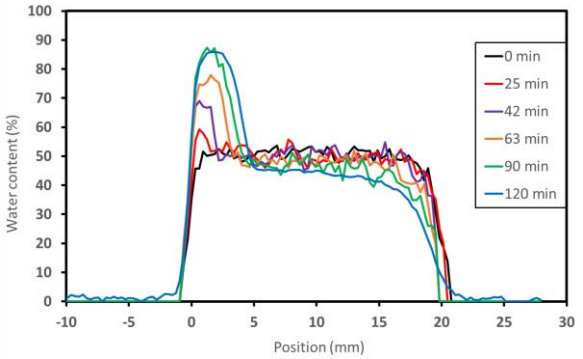

Figure 12 (d): Brine profile measurement at different times in the presence of chemical 4 at 437 ppm (optimal concentration).

From the free water appearance time (Fig. 13), it is apparent that chemical 1 has the lowest concentrations required to resolve water. It starts to level out at 10 ppm, but with an increase to 50 ppm the separation time is reduced to a few minutes. The other chemicals need much higher concentrations to amount to the same separation speed. Chemical 3 has the second fastest separation, also at lower concentrations than the last two, where it reaches a plateau in free water appearance time at around 100 ppm. For the emulsion to experience appearance of free water, chemical 2 must surpass 200 ppm, at which point the appearance time is close to that of chemical 1 and 3. More than 300 ppm of chemical 4 is needed before reaching a plateau, and even at 900 ppm no further decrease occurs. Similar trends arise from the residual water reduction curves at 75% of sample height (Fig.14). The three first chemicals are all able to reduce the free water appearance time below 20 minutes, and the water content to around 20% at a high enough concentrations. Chemical 3 is the only one that shows no sign of a plateau at its highest concentrations. In contrast to chemicals 1-3, chemical 4 has a free water appearance time that levels out at around 60 minutes and is not reduced further at higher concentrations. Similarly, the residual water content plateaus at 40% once a maximum efficiency is reached, which seems to be around 400 ppm for chemical 4.

The emulsified water content (Fig. 15) is minimized to around the same level (≈10%) for chemical 1, 3 and 4; and to a slightly higher level for chemical 2 (≈15%). Chemical 1 is again the most efficient in terms of concentrations necessary to leave as little water in the emulsion as possible, followed by chemical 3, while chemicals 2 and 4 perform similarly as the least efficient. Based on the performances of the four chemicals, the brine profiles have been plotted from each of the optimal concentrations (Fig. 16). An optimal concentration is chosen for each chemical, in which this specific concentration has reached a plateau of residual water content (Fig. 9) and free water layer height (Fig. 10) where further increasing the dosage offers no additional contribution to resolution of water. Chemical 1 and

2 seem to resolve a layer of bulk water at about the same height, but the water content of the emulsified part is slightly lower for chemical 1 as chemical 2 has some additional bumps as an indication of bigger droplets still suspended in the top phase. Chemical 3 clearly has a much higher water content in the emulsified phase at its optimal concentration, and a thinner free water layer than both 1 and 2. Lastly, chemical 4 shows the highest water content in the top and a very thin water layer, thus underperforming compared to the other three chemicals.

The same trends and ranking of efficiencies, as seen in previously mentioned figures, are visible in the free water layer height development over time for the same concentrations of chemicals 1-4 (Fig. 17). Chemical 2 starts off deposition of a free water layer slightly earlier than 1 and 3, but levels out some distance below these (≈ 0.28 H/H_0), whereas 1 and 3 land in the range of 0.32-0.35 H/H_0. As already mentioned, chemical 4 starts developing a continuous water layer no earlier than at around 60 minutes and quickly reaches maximum capacity of free water resolution.

Brine profile comparisons are consistent with the earlier DSD comparison in Figure 11, when considering the top phase of each profile and the DSD intensity level. There appears to be a correspondence between high residual water content and high intensities as well as low residual water and low intensities, and this connection is evident for all the tested chemicals. In addition, chemical 3 has the widest DSD distribution indicating intense coalescence. A high degree of coalescence is also well correlated with its efficiencies (Fig. 13-16), and is the second best tested chemical amongst the four. Free water appearance time curves (Fig. 13) also indicate that slow separation speed in an emulsion results in large residual water contents (Fig. 14 and Fig. 15).

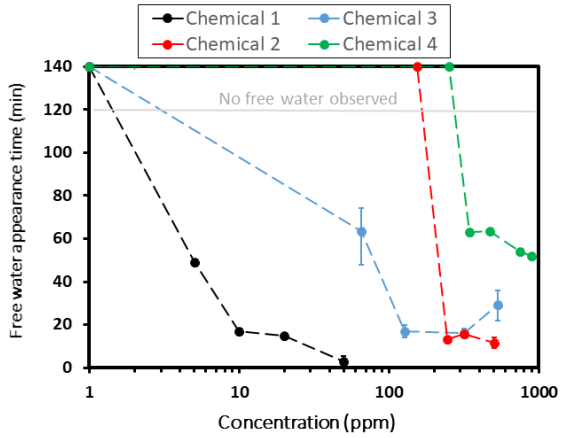

Figure 13: **Free water appearance time (min)** vs. concentration (ppm) of chemicals 1-4 on the logarithmic scale. Chemical 1-4 has two parallels with the average taken. Uncertainties are calculated from the minimum and maximum values. If no free water is observed after 120 minutes of separation then the first value is placed at the top of the figure, above the grey line.

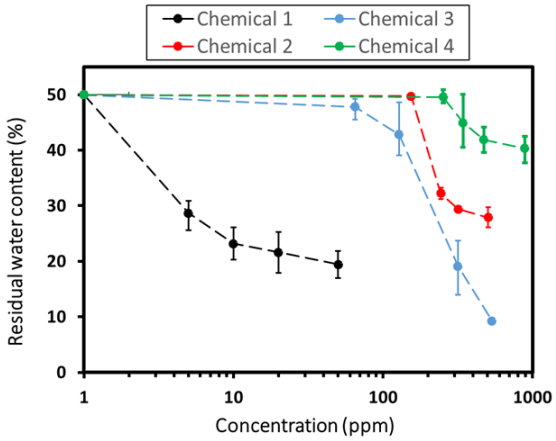

Figure 14: **Residual water cotent (%)** vs. concentration (ppm) for chemicals 1-4 on the logarithmic scale. This is the residual content from 75% of sample height, H/H_0. Chemical #1-4 are all averaged over two parallels per data point. Uncertainties are calculated from the minimum and maximum values.

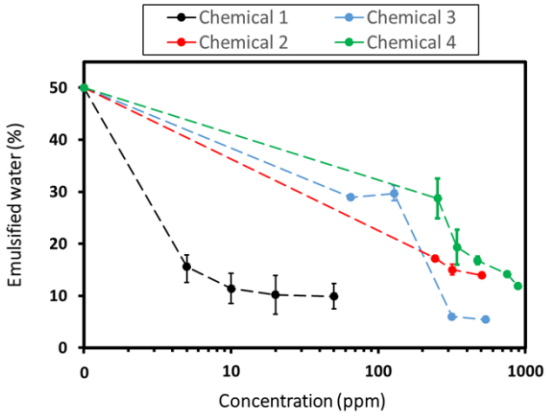

*Figure 15: **Emulsified water (%)** vs. concentration (ppm) of chemicals 1-4 on the logarithmic scale. Emulsified water is droplet signal left after suppression of bulk water signal. Chemical 1-4 has two parallels with the average taken. Uncertainties are calculated from the minimum and maximum values.*

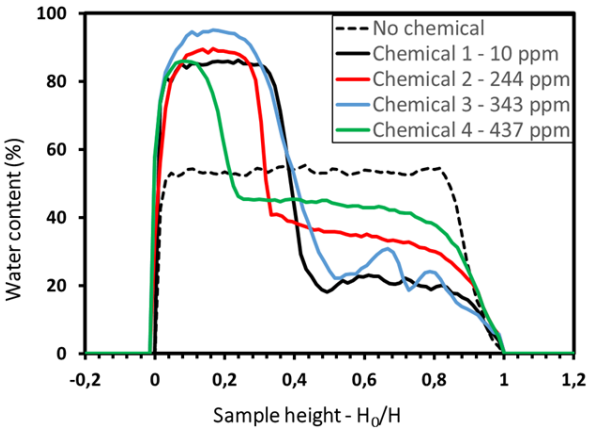

*Figure 16: **Final brine profiles with water content (%)** vs. normalized sample position (H/H_0) for optimal concentrations from each of chemicals 1-4. The final profile for an emulsion containing no chemical is added for reference (black dotted line). One parallel, which is considered representative, of each optimal concentration is shown.*

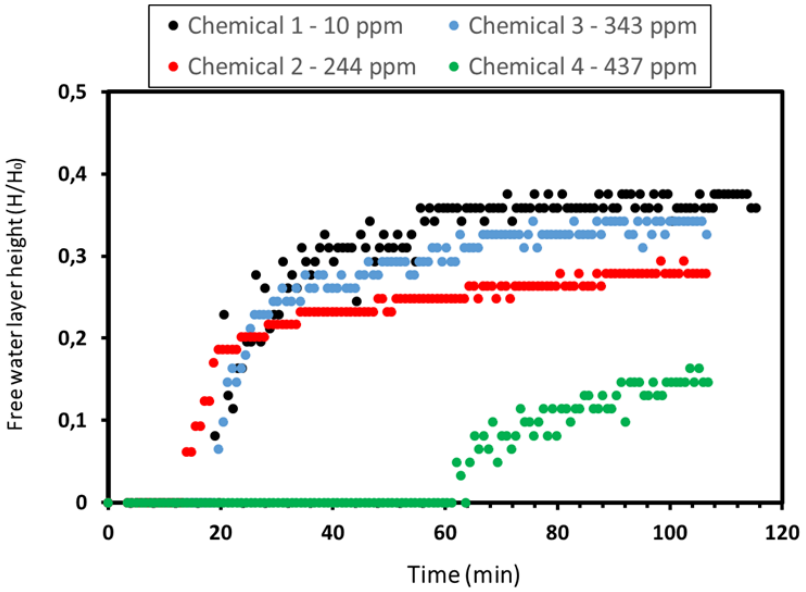

Figure 17: ***Free water layer height (H/H0)*** *vs. time (min) for chemicals 1-4 at their optimal concentrations. This is because of a sensitivity limitation of the NMR.*

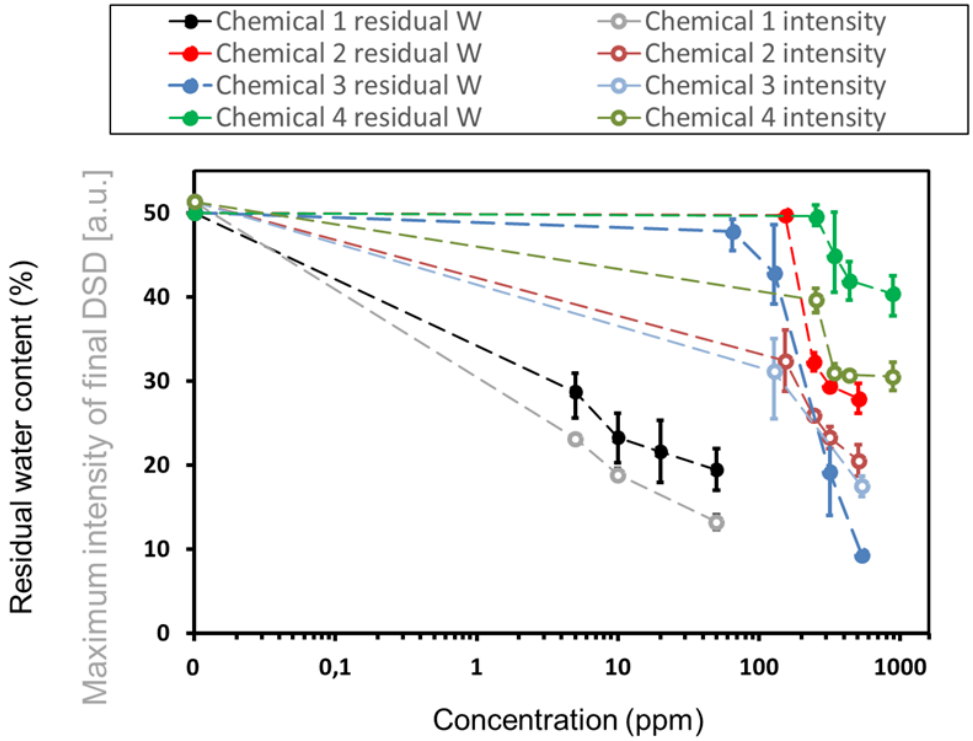

Figure 18: For chemicals 1-4, the ***maximum intensity of final DSD*** *has been plotted on the y-axis vs concentration (ppm) of demulsifier on the x-axis. On the same y-axis,* ***residual water content (%) at 75% of sample height*** *has been plotted vs. concentration (ppm) of demulsifier. The same smoothing factor (=5) and number of scans (=16) has been used for all DSD data to ensure comparability between them. Each data point is the average between two parallels, with error bars representing minimum and maximum values.*

The previously shown results from Figure 14, displaying residual water content, have been plotted together with the maximum intensity of the final DSD at various concentrations of chemicals 1-4 in Figure 18. For all DSD data, the same smoothing factor and the same number of scans has been used to make sure that the receding intensity can be attributed to a decrease in water content. Trends for both the intensity and water content generally show good correlation with each other for all the

chemicals. Maximum intensity of final DSD is decreasing with increasing concentration of chemicals, which also seems to be the case for residual water content in the top phase of the emulsion. Curves representing chemical 1 shows a particularly strong relation between the two aforementioned parameters. Although chemicals 2-4 all have a wider spread between their maximum intensity and residual water curves, the trends are the same. In the case of chemical 4, there is a plateau at around 300 ppm where the intensity of the final DSD stops declining, parallel to the plateau of the residual water content at the same concentration.

4. Discussion

The compared results between chemicals 1-4 shown in the previous sections point towards a ranking of efficiencies lead by chemical 1, in turn followed by 3, 2 and 4, in that respective order. As indicated by Table 2, chemicals 1 and 2 are blends of several components, while chemicals 2 and 4 are single components. These blends have the advantage of containing more components, increasing the chances of being applicable to the specific emulsion system used in these experiments. Whereas the success of the signal component chemicals depend on how compatible they are with regards to certain conditions and parameters related to the emulsion. Although interfacial tension effects have not been documented for chemicals 1-4 in this article, both the reduction of residual (Fig 14.) and emulsified content (Fig. 15) suggest that higher dosages of the chemicals 2-4 are needed at the droplet surface to successfully replace surface active components from the crude oil that may keep droplets from coalescing. However, none of the chemicals are able to completely dry out the emulsion to leave two separate phases, but rather seem to reach a limit of a free water layer height unable to surpass 0.4 H/H_0. The free water layer height limit is also evident for the most efficient chemical. The same goes for the residual water content that tends to cease decreasing at around 20%, even for high concentrations of all chemicals tested here. Since such high dosages have been investigated to reach limitations in resolved water, other parameters may be altered to further the efficiencies of the chemicals tested here; such as the initial droplet sizes of the emulsions for which these chemicals may not have been intended. In addition, the full information on the structure of the chemicals have not been disclosed, limiting our discussion to speculation on the underlying cause of the separation limits observed in these experiments.

The blend referred to as chemical 1, having shown the most promising results, was discussed in the previous section as too fast in coalescing droplets from small to bigger ones that would then quickly leave the top phase. Big droplets are considered indispensable to achieve complete separation as their function is to “catch” the smaller droplets. They also decrease droplet coalescence time compared to when small droplets are in the process of coalescing due to a higher stability of small droplets [44]. Chemicals 2-4 showed slower droplet sedimentation than chemical 1, but their mechanisms to achieve drop-drop coalescence seems somewhat different as neither had any observable sedimentation fronts, as seen from Figures 12 (a)-(b). The non-existent sedimentation front could be a result of longer coalescence time between droplets than for chemical 1, perhaps because the interfacial components within the chemicals are less effective at replacing or competing for space with the crude components at the complex droplet interfaces.

Chemical 3 reaches an emulsified water content in the 10% range for its highest concentration (Fig. 15), which is close to that of chemical 1. However, brine profiles showed around 10% in the upper most part, while the water content in the area right above bulk water was around 40%. It is likely that these water contents are a result of the specific regions containing either predominantly small droplets or big droplets. Therefore, this two-fold divide in water content in the sample, above bulk water, indicates that the top contains very small droplets, while bigger droplets stay suspended close to bulk water, but does not coalesce with it. The NMR suppression method to capture the emulsified

profile seems to suppress the big droplets within the region of 40% water content so that only the part containing 10% water is returned. Therefore, at concentrations of around 500 ppm of chemical 3, the emulsified water content becomes even lower than for chemical 1, while in reality it is due to a limitation of this specific NMR method.

In conclusion, oil-water separation can be followed accurately with modern NMR procedures. The method previously described in this article was specifically developed for the study allowing for measurements of:

(1) Droplet size distributions at the beginning and the end of separation. The final DSD measured only in the top part of the sample to avoid artefact measurements arising due to the presence of free water. The top section measurement allows for determination of the DSD of the residual water droplets that remain in the separated oil phase.
(2) Brine profiles provides the possibility to characterize the sedimentation rate, the residual water content at the top of the emulsion, and the free water appearance kinetic. With all these parameters accurate data can be obtained about patterns of sedimentation and coalescence. Information about the mechanism can also be deducted from brine profiles. Here it was shown that an emulsion in presence of either of the chemicals 2, 3 and 4 do not possess any sedimentation front. The reason behind is not completely understood, but it was noticed that this phenomena appeared for the three least efficient chemicals.
(3) Emulsified water profile determination allows to pinpoint the location of the small to medium sized droplets and, by studying the difference with the total water content of the initial profile, deduction can be made on where bigger droplets and free water layer is.
(4) Finally, as for the specific chemicals tested in this study, the blends (chemicals #1 and #3) were the most efficient for separation of water from the North Sea heavy crude oil. It was sufficient to use lower concentrations for #1 and #3 compared to the other chemicals, while the single components (chemical #2 and #4) were less efficient with higher concentrations needed to reach similar amounts of separated water.

5. Conclusion

Demulsification of crude oil emulsions by means of chemical demulsifiers were followed by a newly developed, next generation NMR procedure. Droplet size distributions, with slice selections, and brine profiles were obtained from emulsions immediately after addition of emulsion breaker, as well as at the end of each experiment. By combining the aforementioned techniques with continuous brine profiles throughout the experiment, it was possible to study how demulsifiers affected coalescence, sedimentation patterns and sedimentation kinetics of the emulsion. From this procedure, a clear ranking of demulsifier separation efficiency emerged, with indications of their mechanisms at play.

Acknowledgements

The authors thank the JIP Electrocoalesence consortium, New Strategy for Separation of Complex Water-in-Crude Oil Emulsions: From Bench to Large Scale Separation (NFR PETROMAKS), consisting of Ugelstad Laboratory (NTNU, Norway), University of Alberta (Canada), Swiss Federal Institute of Technology in Zurich (Switzerland), Institutt for energiteknikk (Norway) and funded by Norwegian Research Council (Grant 255174) and the following industrial sponsors: AkzoNobel, Anvendt Teknologi AS, NalcoChampion, Equinor, and Sulzer.

Supplementary Materials. Further explanation of the theory behind the NMR droplet size distribution calculations and slice selection method, as well as NMR parameter tables, NMR sequences, chemical concentrations and sedimentation rate calculations are supplied as Supplementary Materials.

Numenclature

g = gravitational acceleration, m s^{-2}
NMR = nuclear magnetic resonance
B = external magnetic field
B_0 = magnetic field generated by permanent magnet
G = magnetic field gradient generated by gradient coils
z = position along the z-axis
γ = gyromagnetic ratio
ω = frequency
PFG = pulsed field gradient
STE = stimulated echo
SE = spin echo
RF = radio frequency
DSD = droplet size distribution
$\frac{\overline{S}}{V}$ = average surface-volume ratio
T_1 = spin-lattice relaxation time
T_2 = spin-spin relaxation time
D(t) = restricted time-dependent diffusion coefficient
D_0 = unrestricted diffusion coefficient
t = observation time, s
GS1 = spoiler gradient strength
g, f (Fig. 1) = gradient strength
δ = gradient time duration
δ_1, δ_2 = time intervals before and after gradient
τ = inter-echo spacing
Δ_1 = z-storage delay
Δ_2 = eddy current delay
MW = molecular weight
RSN = relative solubility number
rpm = rounds per minute
ppm = parts per million
WC = water cut, % v/v
V = sedimentation rate, mm/s
R = droplet radius, m
R_{cavity} = dropet cavity radius, m
d = droplet diameter, m
$\boldsymbol{\rho}$ = density, kg/m^3
μ = viscosity, mPa
H_0 = sample height, mm
a = slope of straight line

6. References

(1) Sjöblom, J.; Aske, N.; Harald Auflem, I.; Brandal, Ø.; Erik Havre, T.; Sæther, Ø.; Westvik, A.; Eng Johnsen, E.; Kallevik, H., Our current understanding of water-in-crude oil emulsions.: Recent characterization techniques and high pressure performance. *Adv. Colloid Interface Sci.* **2003,** 100-102, 399-473.

(2) Zhang, J.; Tian, D.; Lin, M.; Yang, Z.; Dong, Z., Effect of resins, waxes and asphaltenes on water-oil interfacial properties and emulsion stability. Colloids Surf., A **2016,** 507, 1-6.

(3) Yin, X.; Kang, W.; Zhao, Y.; Liu, J.; Yang, H.; Dai, C.; Sarsenbekuly, B.; Aidarova, S.; Yang, L.; Yuan, H.; Tan, J., Study on the indigenous stabilization mechanism of light crude oil emulsions based on an in situ solvent-dissolution visualization method. Colloids Surf., A **2017,** 530, 155-163.

(4) McLean, J. D.; Kilpatrick, P. K., Effects of Asphaltene Solvency on Stability of Water-in-Crude-Oil Emulsions. *J. Colloid Interface Sci.* **1997,** 189, (2), 242-253.

(5) Hirasaki, G. J.; Miller, C. A.; Raney, O. G.; Poindexter, M. K.; Nguyen, D. T.; Hera, J., Separation of Produced Emulsions from Surfactant Enhanced Oil Recovery Processes. *Energy Fuels* **2011,** 25, (2), 555-561.

(6) Sams, G. W.; Zaouk, M., Emulsion Resolution in Electrostatic Processes. *Energy Fuels* **2000,** 14, (1), 31-37.

(7) Fan, Y.; Simon, S.; Sjöblom, J., Chemical Destabilization of Crude Oil Emulsions: Effect of Nonionic Surfactants as Emulsion Inhibitors. *Energy Fuels* **2009,** 23, 4575-4583.

(8) Zhang, W.; Xiao, P.; Wang, D., Central treatment of different emulsion wastewaters by an integrated process of physicochemically enhanced ultrafiltration and anaerobic–aerobic biofilm reactor. *Bioresour. Technol.* **2014,** 159, 150-156.

(9) Zhang, H.; Fang, S.; Ye, C.; Wang, M.; Cheng, H.; Wen, H.; Meng, X., Treatment of waste filature oil/water emulsion by combined demulsification and reverse osmosis. *Sep. Purif. Technol.* **2008,** 63, (2), 264-268.

(10) Amarzguioui, M.; Jacobsen, P. C., Novel use of Electro Coalescence to Enhance, Optimize and Debottleneck Oil Separation Trains. In *SPE Annual Technical Conference and Exhibition, 28-30 September*, Soc. Pet. Eng.: Houston, Texas, SPE-174763-MS, 2015.

(11) Rajaković, V.; Skala, D., Separation of water-in-oil emulsions by freeze/thaw method and microwave radiation. *Sep. Purif. Technol.* **2006,** 49, (2), 192-196.

(12) Opedal, N. v. d. T.; Kralova, I.; Lesaint, C.; Sjöblom, J., Enhanced Sedimentation and Coalescence by Chemicals on Real Crude Oil Systems. *Energy Fuels* **2011,** 25, (12), 5718-5728.

(13) Barrabino, A.; Keleşoğlu, S.; Eftekhardadkhah, M.; Simon, S.; Sjöblom, J., Enhanced sedimentation and coalescence of petroleum crude oil emulsions by the new generation of environmentally friendly yellow chemicals. *J. Dispersion Sci. Technol.* **2017,** 38, (12), 1677-1686.

(14) Jones, T. J.; Neustadter, E. L.; Whittingham, K. P., Water-In-Crude Oil Emulsion Stability And Emulsion Destabilization By Chemical Demulsifiers. *J. Can. Pet. Technol.* **1978,** 17, (02), 100-108.

(15) Angle, C. W., Chemical Demulsification of Stable Crude Oil and Bitumen Emulsions in Petroleum Recovery-A Review. In *Encyclopedic Handbook of Emulsion Technology*, Sjoblom, J., Ed. Mercel Dekker: New York, 2001; pp 541-594.

(16) Sjöblom, J.; Johnsen, E. E.; Westvik, A.; Ese, M.-H.; Djuve, J.; Auflem, I. H.; Kallevik, H., Demulsifiers in The Oil Industry. In *Encyclopedic Handbook of Emulsion Technology*, Sjöblom, J., Ed. CRC Press Boca Raton 2001; Vol. 1st Edition, pp 595-619.

(17) Sjöblom, J.; Mingyuan, L.; Höiland, H.; Johansen, E. J., Water-in-crude oil emulsions from the norwegian continental shelf part III. A comparative destabilization of model systems. Colloids Surf. **1990,** 46, (2), 127-139.

(18) Aveyard, R.; Binks, B. P.; Fletcher, P. D. I.; Lu, J. R., The resolution of water-in-crude oil emulsions by the addition of low molar mass demulsifiers. *J. Colloid Interface Sci.* **1990,** 139, (1), 128-138.

(19) Urdahl, O.; Movik, A. E.; Sjöblom, J., Water-in-crude oil emulsions from the Norwegian continental shelf 8. Surfactant and macromolecular destabilization. Colloids Surf., A **1993,** 74, (2), 293-302.

(20) Roodbari, N. H.; Badiei, A.; Soleimani, E.; Khaniani, Y., Tweens demulsification effects on heavy crude oil/water emulsion. *Arabian J. Chem.* **2016,** 9, S806-S811.

(21) Hajivand, P.; Vaziri, A., Optimization of demulsifier formulation for separation of water from crude oil emulsions. Braz. J. Chem. Eng. **2015,** 32, 107-118.

(22) Wang, J.; Hu, F.-L.; Li, C.-Q.; Li, J.; Yang, Y., Synthesis of dendritic polyether surfactants for demulsification. *Sep. Purif. Technol.* **2010,** 73, (3), 349-354.

23. Adilbekova, A. O.; Omarova, K. I.; Karakulova, A.; Musabekov, K. B., Nonionic surfactants based on polyoxyalkylated copolymers used as demulsifying agents. Colloids Surf., A **2015,** 480, 433-438.

(24) Kang, W.; Yin, X.; Yang, H.; Zhao, Y.; Huang, Z.; Hou, X.; Sarsenbekuly, B.; Zhu, Z.; Wang, P.; Zhang, X.; Geng, J.; Aidarova, S., Demulsification performance, behavior and mechanism of different demulsifiers on the light crude oil emulsions. Colloids Surf., A **2018,** 545, 197-204.

(25) Liu, J.; Huang, X.-f.; Lu, L.-j.; Li, M.-x.; Xu, J.-c.; Deng, H.-p., Turbiscan Lab® Expert analysis of the biological demulsification of a water-in-oil emulsion by two biodemulsifiers. *J. Hazard. Mater.* **2011,** 190, (1), 214-221.

(26) Tanner, J. E.; Stejskal, E. O., Restricted Self-Diffusion of Protons in Colloidal Systems by the Pulsed-Gradient, Spin-Echo Method J. Chem. Phys. **1968,** 49, (4), 1768-1777

(27) Packer, K. J.; Rees, C., Pulsed NMR studies of restricted diffusion. I. Droplet size distributions in emulsions. *J. Colloid Interface Sci.* **1972,** 40, (2), 206-218.

(28) Balinov, B.; Urdahl, O.; Söderman, O.; Sjöblom, J., Characterization of water-in-crude oil emulsions by the NMR self-diffusion technique. Colloids Surf., A **1994,** 82, (2), 173-181.

(29) Opedal, N. v. d. T. NMR as a tool to follow destabilization of water-in-oil emulsions (PhD Thesis). NTNU, Trondheim, 2011.

(30) Simon, S.; Pierrard, X.; Sjöblom, J.; Sørland, G. H., Separation profile of model water-in-oil emulsions followed by nuclear magnetic resonance (NMR) measurements: Application range and comparison with a multiple-light scattering based apparatus. *J. Colloid Interface Sci.* **2011,** 356, (1), 352-361.

(31) Sandnes, R.; Simon, S.; Sjöblom, J.; Sørland, G. H., Optimization and validation of low field nuclear magnetic resonance sequences to determine low water contents and water profiles in W/O emulsions. Colloids Surf., A **2014,** 441, 441-448.

(32) Sørland, G. H. In *Characterization of Emulsions by PFG-NMR* The 10th International Bologna Conference on Magnetic Resonance in Porous Media, 12-16 September, Leipzig, Germany, 2010; Leipzig, Germany, 2010; pp 27-31.

(33) Sørland, G. H., *Dynamic Pulsed-Field-Gradient NMR*. Springer-Verlag Berlin Heidelberg: Heidelberg, New York, Dondrecht, London, 2014; Vol. 110.

(34) Opedal, N. v. d. T.; Sørland, G.; Sjöblom, J., Methods for Droplet Size Distribution Determination of Water-in-Oil Emulsions using Low-Field NMR. *diffusion-fundamentals.org* **2009,** 9, (7), 1-29.

(35) Simon, S.; Nenningsland, A. L.; Herschbach, E.; Sjöblom, J., Extraction of Basic Components from Petroleum Crude Oil. *Energy Fuels* **2009,** 24, 1043-1050.

(36) OSPAR OSPAR Decisions, Recommendations & Agreements.

(37) Mitra, P. P.; Sen, P. N.; Schwartz, L. M., Short-time behavior of the diffusion coefficient as a geometrical probe of porous media. *Phys. Rev. B* **1993,** 47, (14), 8565-8574.

(38) Hirasaki, A. P. G., NMR Characterization of Emulsions. In *Emulsions and Emulsion Stability*, Sjöblom, J., Ed. Tailor & Francis Group: New York, 2006; Vol. 2nd Edition, pp 283-304.

(39) Sørland, G. H., Analysis of Dynamic NMR Data. In *Dynamic Pulsed-Field-Gradient NMR*, Sørland, G. H., Ed. Springer Berlin Heidelberg: Berlin, Heidelberg, 2014; pp 129-168.

(40) Yeung, A.; Dabros, T.; Czarnecki, J.; Masliyah, J., On the interfacial properties of micrometre–sized water droplets in crude oil. *The Royal Society* **1999,** 455, (1990), 3709-3723

(41) Masliyah, J. H.; Xu, Z.; Dabros, M.; Czarnecki, J. A., 7.4. Demulsifiers and Other Chemical Aids. In *Handbook on Theory and Practice of Bitumen Recovery from Athabasca Oil Sands*, Kingsley Publishing Services:: Cochrane, Alberta, 2011; Vol. 5th.

(42) Pradilla, D.; Simon, S.; Sjöblom, J., Mixed interfaces of asphaltenes and model demulsifiers part I: Adsorption and desorption of single components. Colloids Surf., A **2015,** 466, 45-56.

(43) Mhatre, S.; Simon, S.; Sjöblom, J.; Xu, Z., Demulsifier assisted film thinning and coalescence in crude oil emulsions under DC electric fields. *Chem. Eng. Res. Des.* **2018,** 134, 117-129.

(44) Zolfaghari, R.; Fakhru'l-Razi, A.; Abdullah, L. C.; Elnashaie, S. S. E. H.; Pendashteh, A., Demulsification techniques of water-in-oil and oil-in-water emulsions in petroleum industry. *Sep. Purif. Technol.* **2016,** 170, 377-407.

TOC/abstract graphics